NUMERICAL SIMULATION OF A DELTA WING WITH VORTEX BREAKDOWN USING THE LATTICE BOLTZMANN METHOD

Taro IMAMURA *, Kojiro SUZUKI ** , Takashi NAKAMURA *
*** Japan Aerospace Exploration Agency, Institute of Space Technology and Aeronautics**
**** University of Tokyo, Department of Advanced Energy**

Keywords: *Vortical Flow, Delta Wing, Lattice Boltzmann Method*

Abstract

Investigation of the subsonic flow around a delta wing at high angle-of-attack is essential to meeting the requirements of high-lift-flight for high-speed aircraft during takeoff and landing. Many studies have been dedicated to this problem using experimental and numerical approaches.

Recently, Lattice Boltzmann Method (LBM) has become one of the computational methods to calculate low Mach number flow. Originally, LBM is formulated on isotropic grid such as orthogonal grid with equal spacing. We have extended the LBM to generalized coordinates based on the idea of Interpolation Supplemented LBM (ISLBM). We have validated our code on two-dimensional cases, and results are consistent with the other flow solvers that are based on Navier-Stokes equation and lattice Boltzmann Equation (LBE).

In this paper, a multi-block version of the three-dimensional code was constructed. Before solving delta wing, 3D lid-driven cavity problem was solved as a benchmark problem. The present results are compared with numerical results obtained by Navier-Stokes computations and shows good agreement. Flow around a delta wing with a sweep angle of 76 deg is then solved. Well known flow structures around delta wing, such as separation line on the upper surface, vortex breakdown phenomenon are simulated by the current code.

1 Introduction

Investigation of the subsonic flow around a delta wing at high angle-of-attack is essential to meeting the requirements of high-lift-flight for high-speed aircraft during takeoff and landing. At moderate angles-of-attack, a pair of leeward-side vortices is formed above the upper surface of the delta wing due to the leading-edge flow separation [1]. As the angle-of-attack increases, the leeward-side vortices are strengthened, and sudden bursting of the vortices occurs. This is commonly referred to as vortex breakdown.

Recent advances in computing techniques based on the discretization of the Navier-Stokes equations have made it possible to calculate complicated three-dimensional flowfields [2-4]. Numerical flow simulation has become one of the most important design tools of aerospace vehicles. However, numerical analysis of a flowfield including separation and vortices is still a challenging problem, since artificial viscosity included in the discretization may smear such phenomena.

Recently, the Lattice Boltzmann Method (LBM), which is based on kinetic equations of the particles, has been applied to various low-speed flow simulations [5]. The standard LBM, commonly referred to as the Lattice Bhatnagar-Gross-Krook (LBGK) model, is known to be an efficient and accurate solver for an incompressible flow problem, since it is essentially free from the artificial viscosity due to the Lagrangian procedure of the pseudo particles and does not require time-consuming solution procedure of the Poisson equation for the pressure. Although LBGK is expected to be a good solver for flow problems with separation and vortices, this method still has a few disadvantages that limit its application as a practical CFD tool. One of the limitations is that the grid used in the calculation is required to be

isotropic (e.g, orthogonal coordinates with equal spacing). However, when the Reynolds number is large, clustering the grid nodes around the wall boundary is effective to capture the boundary layer within the limitation of the computational time and storage. In the Generalized form of Interpolation supplemented Lattice Boltzmann Method (GILBM) [6], developed by the current authors, the Lattice Boltzmann equation is transformed into generalized coordinates using grid metrics. The usage of the generalized coordinates enhances the applicability of LGBK for low Mach number flow analysis around a practical configuration at practical Reynolds numbers.

In the present study, the flow around a high angle-of-attack delta wing with vortex breakdown is numerically simulated using GILBM. For the present calculation, a multi-block version of the three-dimensional GILBM was constructed. The present results are compared with numerical results obtained by Navier-Stokes computations.

2 Numerical Methods

2.1 Lattice Boltzmann Method on orthogonal grid system

The LBM describes flows by the collision and advection calculation of distribution functions as follows. The Three-dimensional 15-velocity (3D15V) model is used in the present calculations. The governing equation of the LBM, Lattice Boltzmann Equation (LBE), is described as

$$f_i(\mathbf{x}+\mathbf{c}_i\Delta t, t+\Delta t) - f_i(\mathbf{x},t) = -\frac{1}{\omega}\left[f_i(\mathbf{x},t) - f_i^{(eq)}(\mathbf{x},t)\right], \quad (1)$$

where $i = 0,1,2\cdots,14$. f_i and $f_i^{(eq)}$ are the distribution function and the equilibrium distribution function corresponding to the discrete velocity vector $\mathbf{c}_i$, respectively. The value Δt is the time step and ω is the relaxation time. The right and left hand sides of Eq.(1) corresponds to the collision and the advection terms, respectively. Thus Eq.(1) can be divided into two phases as

$$f_i^*(\mathbf{x},t) = -\frac{1}{\omega}\left[f_i(\mathbf{x},t) - f_i^{(eq)}(\mathbf{x},t)\right]$$

: Collision term, (2)

$$f_i(\mathbf{x},t+\Delta t) = f_i^*(\mathbf{x}-\mathbf{c}_i\Delta t,t)$$:

Advection term, (3)

where f_i^* indicates the post-collision distribution function. The discrete velocity vector are defined as

$$\left[\mathbf{c}_0^T,\mathbf{c}_1^T,\mathbf{c}_2^T,\mathbf{c}_3^T,\mathbf{c}_4^T,\mathbf{c}_5^T,\mathbf{c}_6^T,\mathbf{c}_7^T,\mathbf{c}_8^T,\mathbf{c}_9^T,\mathbf{c}_{10}^T,\mathbf{c}_{11}^T,\mathbf{c}_{12}^T,\mathbf{c}_{13}^T,\mathbf{c}_{14}^T\right] = c\begin{bmatrix} 0 & 1 & 0 & 0 & -1 & 0 & 0 & 1 & -1 & -1 & 1 & 1 & -1 & -1 & 1 \\ 0 & 0 & 1 & 0 & 0 & -1 & 0 & 1 & 1 & -1 & -1 & 1 & 1 & -1 & -1 \\ 0 & 0 & 0 & 1 & 0 & 0 & -1 & 1 & 1 & 1 & 1 & -1 & -1 & -1 & -1 \end{bmatrix} \quad (4)$$

and the equilibrium distribution function is defined as

$$f_i^{(eq)}(\mathbf{x},t) = w_i\rho\left[1+\frac{3c_{i,\alpha}u_\alpha}{c^2}+\frac{9\left(c_{i,\alpha}u_\alpha\right)^2}{2c^4}-\frac{3u^2}{2c^2}\right], \quad (5)$$

with

$$w_0 = 2/9,$$
$$w_1 = \cdots = w_6 = 1/9,$$
$$w_7 = \cdots = w_{14} = 1/72,$$

for 3D15V model.

The macroscopic variables such as density and velocity are obtained from integrating the moment of the distribution functions over the velocity plane as

$$\rho = \sum_i f_i, \quad \rho\mathbf{u} = \sum_i f_i\mathbf{c}_i. \quad (6)$$

By applying the Chapman-Enskog expansion to the governing equation, the relation between the

LBE (Eq.(1)) and the Navier-Stokes equations is obtained. The relationship between the relaxation time ω and the Reynolds number can be derived as

$$\mathrm{Re} = \frac{6}{(2\omega - 1)\Delta t\, c^2}, \qquad (7)$$

and the pressure is given as $p = \rho c^2 / 3$.

2.2 Generalized form of Interpolation-based Lattice Boltzmann Method

In this section, LBM model on generalized coordinates is introduced based on the idea of ISLBM [7,8]. The physical plane $\mathbf{x}$ is transformed into computational plane described by ξ. Eq.(2) and (3) are transformed into generalized coordinates as follows. The collision term on generalized coordinates is described as

$$f_i^*(\xi, t) = -\frac{1}{\omega}\left[f_i(\xi, t) - f_i^{(eq)}(\xi, t)\right], \qquad (8)$$

where ω, $f_i^{(eq)}(\xi, t)$, and $f_i^*(\xi, t)$ correspond to the relaxation time, the equilibrium distribution function, and the post-collision distribution function, respectively. The advection term is solved as

$$f_i(\xi, t + \Delta t) = f_i^*(\xi - \Delta\xi_{up,i}, t), \qquad (9)$$

where

$$\Delta\xi_{up,i} = \left(\Delta\xi_{up}, \Delta\eta_{up}\right) = \int_0^{\Delta t} d\xi = \int_0^{\Delta t} \tilde{\mathbf{c}}_i \, dt. \qquad (10)$$

This is the time integration of the contravariant velocity. Two-step Runge-Kutta method is used for the integration of Eq.(10) in order to maintain the numerical accuracy in highly clustered grid region. By using the metrics and the discrete velocity $c_{i,\beta}$, the contravariant velocity $\tilde{c}_{i,\alpha}$ is obtained as

$$\tilde{c}_{i\alpha} = c_{i\beta}\frac{\partial \xi_\alpha}{\partial x_\beta}, \qquad (11)$$

where the summation convention is used for the subscript α, β. The right hand side of Eq.(9) should be calculated using second-order upwind multi-dimensional interpolation [7,8]. By introducing the contravariant velocity, the advection term is calculated in the computational space, and the grid is not restricted to any specific grid system for LBM, such as isotropic grids.

2.3 Wall boundary conditions for GILBM

In this study, suitable wall boundary condition for the generalized coordinates is obtained based on the idea of the incompressible Navier-Stokes solvers. The wall boundary condition for the incompressible Navier-Stokes solvers is defined as follows. Since the normal gradient of the pressure vanishes at the wall boundary, pressure on the wall $p_{j=0}$ is extrapolated from the node in the computational domain next to the wall boundary node as $p_{j=0} = p_{j=1}$. In LBM, similar expression for density is obtained as $\rho_{j=0} = \rho_{j=1}$. The flow velocity at the wall is given as wall velocity.

From the boundary condition of the macroscopic variables (ρ, u, v), the boundary condition of the distribution function is calculated. If we assume $f_i \cong f_i^{(eq)}$, distribution function can be calculated using Eq.(5). However, this assumption is not accurate enough since viscosity effect appears in the first-order of non-equilibrium term. The distribution function is estimated up to the first-order of non-equilibrium using the Chapman-Enskog expansion as

$$\begin{aligned} f_i &\cong f_i^{(eq)} + f_i^{(1)} \\ &= f_i^{(eq)}\left[1 - \omega\Delta t\left(\frac{3U_{i\alpha}U_{i\beta}}{c^2} - \delta_{\alpha\beta}\right)\frac{\partial u_\alpha}{\partial x_\beta}\right], \end{aligned} \qquad (12)$$

where $U_{i,\alpha} = c_{i,\alpha} - u_\alpha$, and $\delta_{\alpha\beta}$ is Kronecker delta.

3 Numerical Results

3.1 Three-dimensional Lid-driven Cavity problem

Three-dimensional lid-driven cavity flow calculations are discussed in this section in order to validate the code extended to three-dimension. The flow is driven by the uniform translation of the topside wall, which is defined as $U_{top}/c = 0.1$. The Reynolds number is based on the velocity of the topside wall and the side length of the cavity. For the present calculation, the grid nodes are clustered around the surrounding walls to resolve the boundary layer accurately. The minimum grid spacing around the wall is defined as $\Delta x_{\min} = 0.1/\sqrt{\mathrm{Re}}$. The grid resolutions used in the simulations are 65x65x65 for three cases where Re=100, 400, and 1000.

Figure 1,3 and 5 show the mid-plane cross section streamlines and overall view for Re=100, 400 and 1000. For two-dimensional calculations, secondary vortices were observed at the lower corner for Re=100. However, for three-dimensional cases, the additional vortex does not exist at the corners. Around z=0.2 of the yz-plane for Re=400 in Fig.3, two distinct secondary vortices are found near the corner. These vortices gradually move toward the corners when the Reynolds number increases to 1000. This tendency is also observed in the Navier-Stokes calculations performed by Ku *et al.* [9]. Also, two more small secondary vortices appear at the upper corner of the cavity for Re=1000.

The velocity profiles on the vertical and horizontal centerlines for Re=100, 400, and 1000 are shown in Fig. 2, 4 and 6, respectively. The line indicates the present results; the symbol represents the Navier-Stokes solution [9]. The results for Re=100 and 400 are in good agreement. The results for Re=1000 are rather dissipative compared to the Navier-Stokes results. The grid resolution away from the wall for the present calculation is relatively coarse compared with the Navier-Stokes results, which were obtained on an orthogonal grid with equal spacing. A high-resolution grid is also necessary in the regions away from the walls for these problems.

3.2 Delta Wing

Numerical simulation of the flow around a delta wing with a sweep angle of 76 deg. (an aspect ratio of 1) is performed. The wing geometry is the same as that used in the experiment by Hummel [2]. The Reynolds number based on the macroscopic free stream velocity and the chord length of the delta wing is 9.0×105. All of the calculations were assumed to be laminar. The grids consist of four blocks, and the total number of grid points is 500,000. In order to resolve the vortices accurately, 80% of the grid points are located to the upper side of the wing. The minimum grid size around the wing is defined as $\Delta x_{\min} = 0.1/\sqrt{\mathrm{Re}}$. The grid used in the simulation is shown in Fig. 7.

3.2.1 AOA=20.5[deg] case

The first case is performed at angle-of-attack at 20.5[deg] in order to validate the present code with the experimental results obtained by Hummel [2]. The oil flow pattern of the upper surface is shown in Fig.8. The upper part of the figure is the present result and is compared with the experimental results (lower part). The secondary separation line is observed near the leading edge for both results. The agreement in the location of the separation line is good.

In Fig.9, the pressure and velocity fields of the cross section at x/c=0.5 is shown. The lower figure shows a close-up near the leading edge. The secondary vortex and the separation point are observed. In Fig.10, the computed pressure coefficient distribution of the upper surface is compared with the experiment.

Except for 90% chord distribution, the present results agree qualitatively with the experiment. The negative pressure coefficient peak caused by the secondary separation is also observed around the 90% spanwise location in the computational results.

Figure.11 shows the aerodynamic coefficients vs. angle-of-attack. The pitching moment coefficient C_m (nose-up positive) is defined around the reference point x/c=0.5. They are in good agreement with the experimental results.

3.2.1 AOA=50[deg] case

Simulation at an angle-of-attack 50 deg. was performed to capture the vortex breakdown on the delta wing. Figure 12 shows the instantaneous streamlines over the delta wing. The straight streamlines from the apex show the existence of the vortex core, and the spiral streamlines observed above the aft body indicate the vortex breakdown. The bursting point location x/c=0.5 predicted by the present results, compares well with predictions by the Navier-Stokes equations (x/c=0.4) [3]. These results demonstrate that GILBM has the capability to accurately simulate the vortex breakdown phenomena. and that it will become a useful analysis tool for low-speed high-angle-of-attack flow problems.

4 Conclusions

In order to solve the flow around three-dimensional delta wing configuration, a multi-block version of the three-dimensional generalized form of Interpolation supplemented LBM (GILBM) code was constructed. Before solving delta wing, code validation was performed by solving 3D lid-driven cavity problem and the present results are consistent with the previous study. Using this code, flow around a delta wing with a sweep angle of 76 deg is solved. Well known flow structures around delta wing, such as separation line on the upper surface, vortex breakdown are simulated successfully by the present code.

References

[1] Lambourne, N.C., Bryer, D.W. The Bursting of Leading-Edge Vortices – Some observations and Discussion of the Phenomenon, ARC R\&M 3282.(1961)

[2] Hummel D. “On the Vortex Formation over a Slender Wing at Large Angles of Incidence”, High Angle of Attack Aerodynamics, *AGARD-CP-247*, Paper No.15, (1979)

[3] J.A.Ekaterinaris and Lewis B.Schiff “Numerical Simulation of Incidence and Sweep Effects on Delta Wing Vortex Breakdown”, *Journal of Aircraft* Vol.31, No.5 (1994)

[4] K.Fujii and P.Kutler, Numerical Simulation of the Viscous Flow Fields Over Three-Dimensional Complicated Geometries, AIAA-84-1550 (1984)

[5] S.Chen, G.Doolen, “Lattice Boltzmann Method for Fluid Flows”, *Annu.Rev.Fluid Mech*.1998, 161, pp.329 (1998)

[6] T.Imamura, K.Suzuki, T.Nakamura, Flow simulation Around an Airfoil using Lattice Boltzmann Method on Generalized Coordinates, AIAA paper 2004-0244, 42nd AIAA Reno

[7] X.He, and G.Doolen, Lattice Boltzmann Method on Curvilinear Coordinate System: Flow around a Circular Cylinder, *J. Comput. Phys.* **134** 306 (1997)

[8] Xiaoyi He, Li-Shi Luo, and Micah Dembo, Some Progress in Lattice Boltzmann Method. Part 1. Nonuniform Mesh Grids, *J. Comput. Phys.* **129** 357 (1996)

[9] Hwar C. Ku, Richard S. Hirsh, and Thomax D. Taylor, A Pseudospectral Method for Solution of the Three-dimensional Incompressible Navier-Stokes Equations, *J. Comput. Phys.* **70**, 439 (1987)

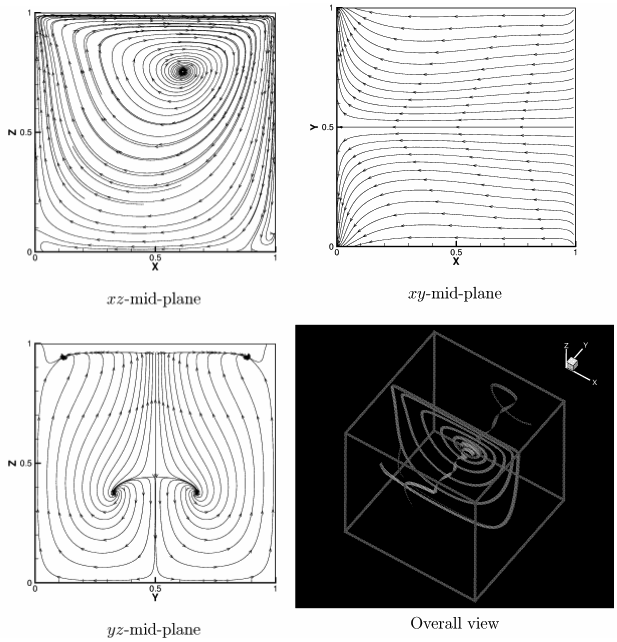

Figure 1 : Three dimensional cavity simulation at Re=100

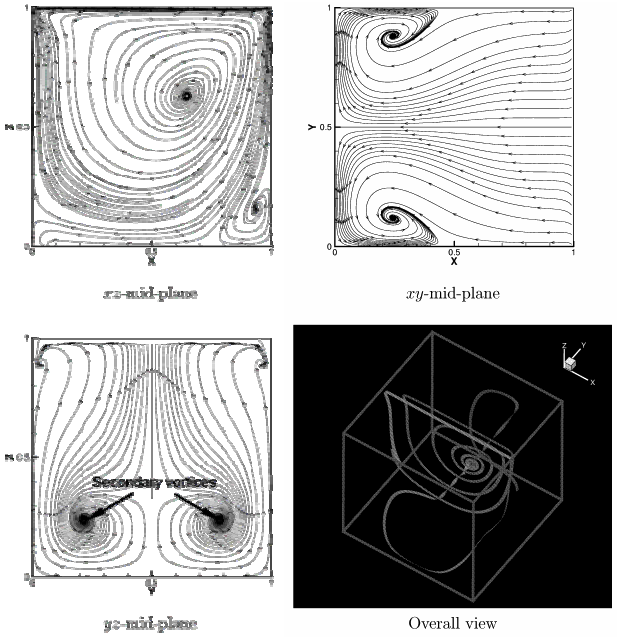

Figure 3 : Three dimensional cavity simulation at Re=400

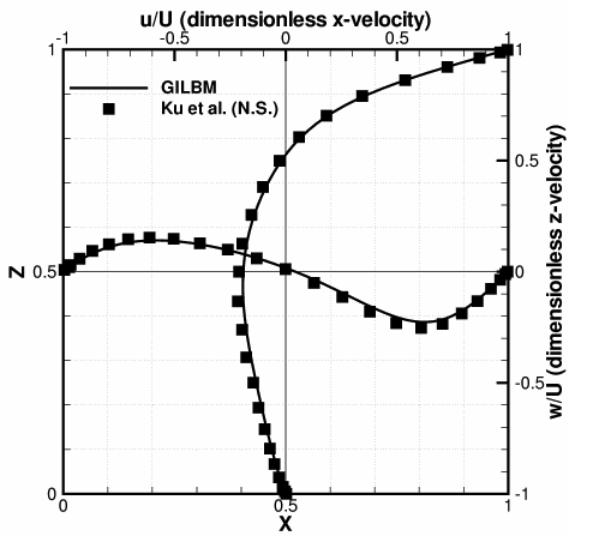

Figure 2 : Velocity profiles for Re=100 on vertical centerline and horizontal centerline

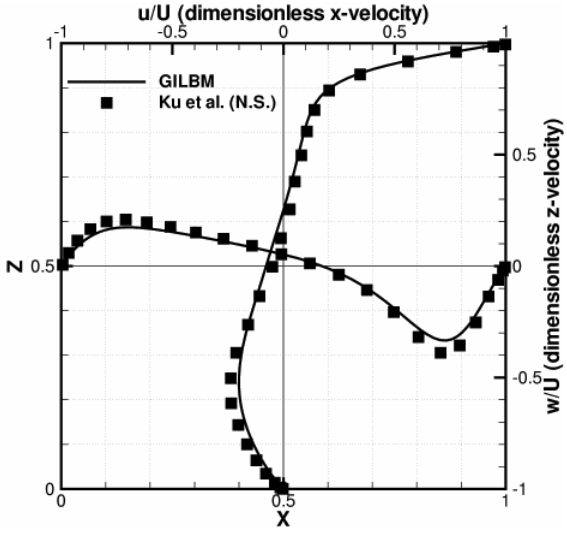

Figure 4 : Velocity profiles for Re=400 on vertical centerline and horizontal centerline

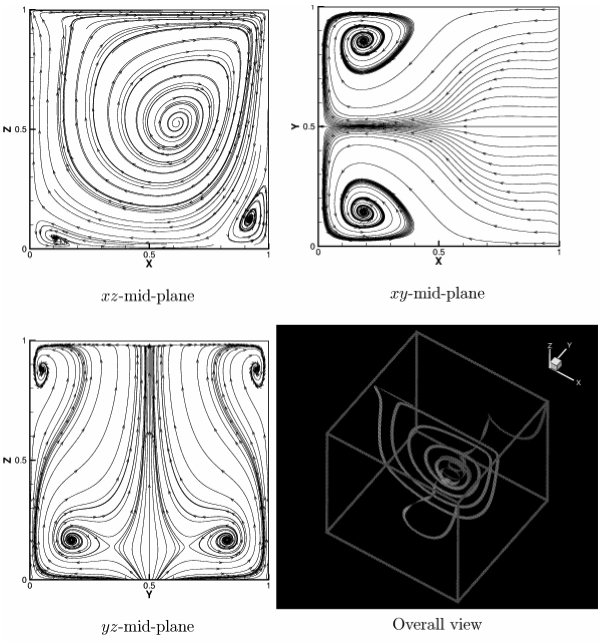

Figure 5 : Three dimensional cavity simulation at Re=1000

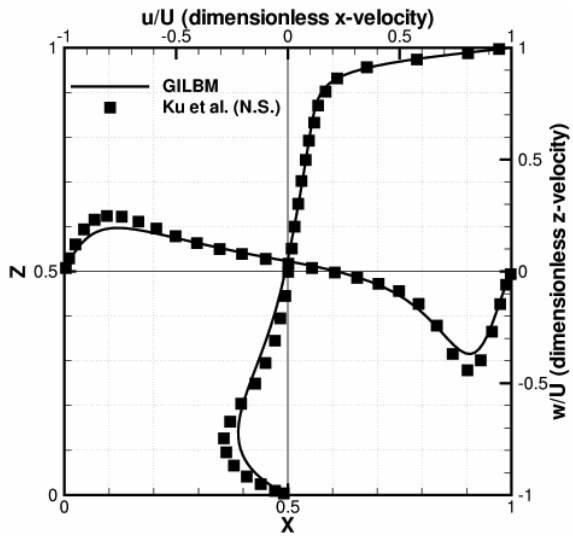

Figure 6 : Velocity profiles for Re=1000 on vertical centerline and horizontal centerline

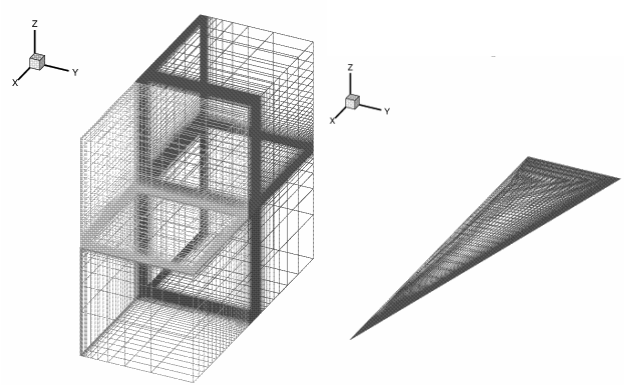

Figure 7 : Computational grid and surface grid for the Delta wing configuration

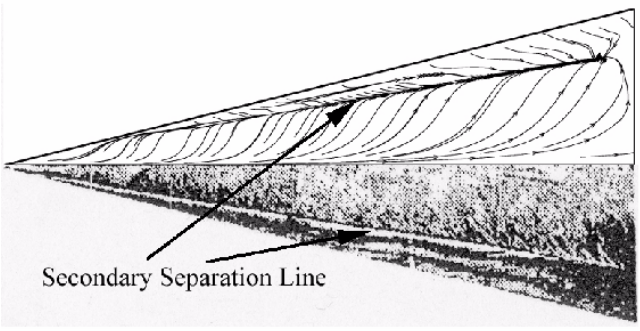

Figure 8: Surface oilflow patterns
Upper : Current result
Lower : Experiment by Hummel [2]

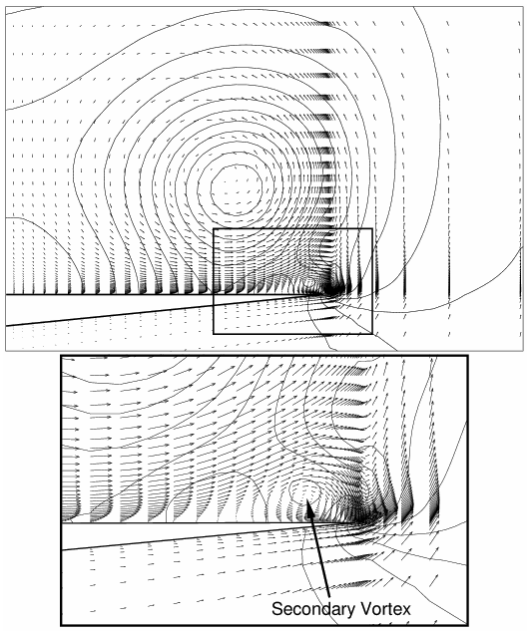

Figure 9: Computed pressure and velocity field in cross flow plane at x/c=0.5

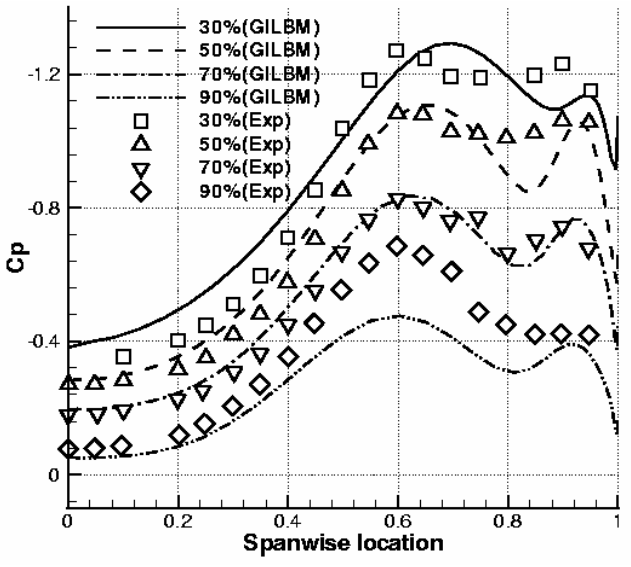

Figure 10: Comparison of Cp distribution with the experiment at AOA=20.5[deg]

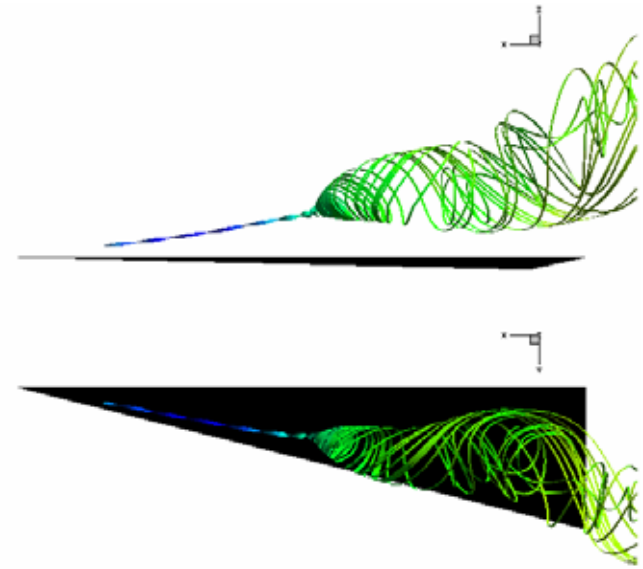

Figure 12: Surface pressure distribution and the streamlines from the apex
(upper: side view lower: top view)

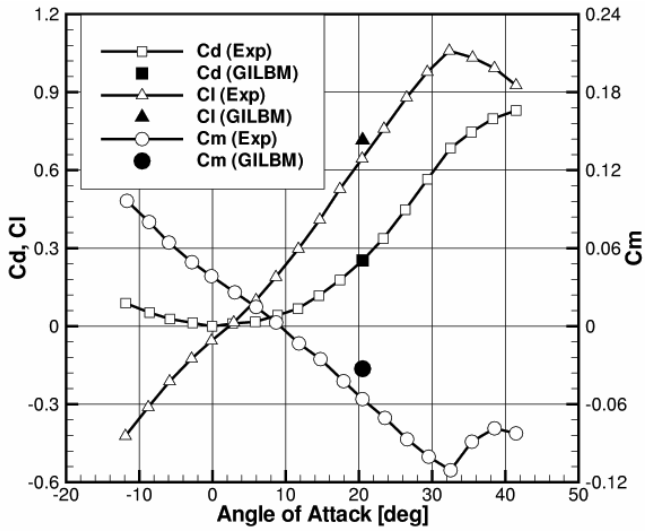

Figure 11: Aerodynamic coefficients vs. angle-of-attack